Section A-Research Paper
ISSN 2063-5346

CFD Analysis of U-Shaped Vertical Ground Coupled Heat Exchanger Under Various Soil Surface Condition with Experimental Validation

Gajendra Kumar*, Radha Krishna Prasad, and Ram Vinoy Sharma
Department of Mechanical Engineering, NIT Jamshedpur, Jharkhand, INDIA, 831014
Corresponding Author*: 2015rsme003@nitjsr.ac.in
Mobile No.: +916205367414

Article History: Received: 06.04.2023 Revised: 25.05.2023 Accepted: 05.06.2023

Abstract

This investigation examines the performance of a U-shaped vertical ground-coupled heat exchanger (VGCHE) under a range of soil conditions. A three-dimensional model of a Ushaped tube with a diameter of 0.0254 meters and a depth of 17 meters was developed to replicate the heat transfer process. The CFD model is solved with the assistance of the Finite Volume Method (FVM), which employs a range of different intake water flow rates. The temperature of the soil is predicted by a model of convective heat transfer between the surface of the soil and the air surrounding it to change in tandem with the surface temperature of the soil. An experiment was carried out at the National Institute of Technology Jamshedpur in India to offer evidence for the dynamic thermal behavior of the VGCHE under a range of soil surface conditions. During hot summer days the performance of VGCHE is efficient under wet sheltered condition when soil act as a heat sink and during cold winter days dry sunlight condition is most suitable for VGCHE when the soil act as a heat source. It is often utilized in residential, commercial, and industrial buildings for the production of hot water in addition to the heating and cooling of the interior.

Keywords: Ground heat exchanger, CFD analysis, U-Shaped Tube, Soil Surface conditions, Finite volume method.

DOI: 10.53555/ecb/2022.11.6.133

Nomenclature

VGCHE	:	Vertical ground couple heat exchanger
CFD	:	Computation fluid dynamics
FVM	:	Finite volume method
GHE	:	Geothermal heat exchangers
T	:	Earth Temperature [K]
T_e	:	Effective temperature [K]
t	:	Time [s]
y	:	Depth from earth surface [m]
α	:	Thermal diffusivity [$m^2.S^{-1}$]
K	:	Thermal conductivity [$W.m^{-1}. K^{-1}$]

CE : Convective energy [W]
LR : Long wave emissive radiation [$W.m^{-2}$]
SR : Soil radiation [$W.m^{-2}$]
LE : Latent heat flux due to evaporation [$W.m^{-2}$]
h_s : Total transmission of heat coefficient for soil surface [$W.m^{-2}. K^{-1}$]
h_c : Transmission of heat due to convection coefficient [$W.m^{-2}. K^{-1}$]
h_r : Radiative transmission of heat coefficient [$W.m^{-2}. K^{-1}$]
h_e : Effective transmission of heat coefficient [$W.m^{-2}. K^{-1}$]
ε : Emittance of earth surface
v : Velocity of air [$m.s^{-1}$]
σ : Stefens Boltzmann constant [$W.m^{-2}. K^{-4}$]
m_e : Soil surface mass evaporation [$Kg. s^{-1}$]
L : Latent heat of vaporization [$KJ. Kg^{-1}$]
P_S : Saturated water vapor pressure [Pa]
γ : Relative humidity
f : Evaporation rate coefficient
α_0 : Soil surface absorptivity
c_p : Specific heat capacity [$KJ. Kg^{-1}. K^{-1}$]
ρ : Density of soil [$Kg.m^{-3}$]
Ψ : Phase difference
ω : 2Π/time [$rad. s^{-1}$]
ρ : Density of fluid [$kg.m^{-3}$],
$\vec{v}$: Velocity vector in [$m.s^{-1}$].
p : Static pressure [$N.m^{-2}$],
$\bar{\tau}$: Surface shear stress [$N.m^{-2}$]
$\rho\vec{g}$: Gravitational body force [N]
$\vec{F}$: External body force in [N] k :
Turbulent kinetic energy per unit mass [$J.kg^{-1}$]
ε : Rate of dissipation of turbulent kinetic energy per unit mass [$m^2.s^{-3}$]
S_k : Source terms
σ_ε, σ_k : Prandtl numbers of k and ε μ_t :
Eddy viscosity [$m^2.s^{-1}$]
v : Fluid velocity [$m.s^{-1}$].

Subscript
0 : First term of Fourier series
m : Number of terms
e : Effective
a : Ambient

1. Introduction

India's buildings are responsible for 20% of the country's overall energy consumption, with residential and commercial buildings each accounting for 10%. In homes, energy use for fans and air conditioning systems is 41%, while in businesses it is 34% due to air conditioning alone. By 2030, experts predict that both the demand for and the installed base of air conditioners will have increased three times. Residential air conditioning is expected to account for 85% of all floor space in India by 2050 as urbanization and the country's economy grow. As a result of their efficiency and low impact on the environment, VGCHE (vertical ground-coupled heat exchanger) systems have gained traction as a viable option for dealing with this issue. Understanding the heat carrier fluid temperature and keeping the ground and fluid from overheating during system operation via the U-shaped tubes and heat pump necessitates a thermal analysis of the ground heat exchanger.

Unpredictable factors like groundwater flow, thermal characteristics, and construction weight make VGCHE heat transfer more challenging. The literature offers various experimental, numerical, and analytical approaches and responses. Due to its intricacy and size over time, the heat transmission mechanism is often examined in two zones. Heat conduction in solid soil or rock beyond the borehole is transitory. In specific operational conditions, the earth's thermal reaction can detect borehole wall temperature at any moment. These assessments ensure that the ground and fluids moving through it never exceed safe temperatures, improving energy efficiency and environmental sustainability. A complete investigation of a borehole must check both its inside (containing grout, U-shaped tube tubes, and circulating fluid) and exterior (containing merely solid earth or rock). Evaluations typically designate the inner area as steady-state or transient because of its potential impact on borehole wall performance.

Ground thermal characteristics and temperature greatly impact ground-coupled heat exchanger design and analysis. Climate change complicates soil temperature fluctuations. However, ground temperature and depth are thought to be sinusoidal. Understanding how ground temperature affects the ground-coupled heat exchanger is crucial [1]. As one descends within the Earth, temperature change slows until equilibrium. Several surface energy balance studies have been conducted. Solar radiation affects the Earth's atmosphere's temperature over extended periods and at deep depths [2]. We now understand how solar radiation affects Earth's surface energy balance. Kuwaiti seasonal and diurnal temperature swings have been studied using the equation. We utilize the surface energy balance as a boundary condition to study how land affects Earth's surface temperature [3], [4]. Several investigations have demonstrated that Earth's boundary conditions are the sun's rays, heat loss to the frigid sky via long-wavelength solar radiation, convectional heat transfer from the atmosphere to the surface, and soil moisture evaporation. The energy balance equation considers several elements that affect energy flow from the atmosphere to the soil. Evaporation's latent heat flow, Earth's long-wave radiation, solar absorption, and convective energy exchange are examples [5]. Air temperature, wind speed, and sun radiation can calculate the effective temperature. The soil's shade or sunlight can also affect its temperature. The energy balance equation shows how several factors affect Earth's average temperature.

Analytical geothermal heat exchanger models began with the infinite line source model, which uses geometry approximations. This model assumes a constant soil temperature throughout the borehole, which is shown as a virtually unending line. Integration solves borehole ambient temperature problems. Ingersoll and Plass [6] implemented this idea in 1948, and Eskilson [7] enhanced it subsequently. Despite its shortcomings, the infinite line source model advanced geothermal heat exchanger analytical models. Cimmino et al. [8] used the analytical finite line source approach to handle buried depth-to-height ratios and borehole heat extraction rate variations. This augmentation was considered, unlike Eskilson's previous investigations. The infinite cylindrical source model used to solve the heat equation imposes a heat flow condition on the surface to determine the borehole diameter temperature. Beier [9] solved numerous heat conduction problems using Laplace transformations. These models have improved our ability to analyze geothermal heat transmission. Despite differences in technique and outcomes, these models provide improved analytical tools for geothermal heat exchange. Numerical simulation allows researchers to manipulate boundary conditions, operating parameters, design factors, and system configurations to better understand geothermal heat exchangers and complex systems.

Eskilson [10] recommended a two-dimensional explicit finite difference technique (GHE) to detect soil temperature near a ground heat exchanger. Eskilson's g-function and curves can characterize borehole performance depending on the bore field layout. Dimensionless temperature response factor g-function Hellstrom [11] computed vertical ground heat exchanger efficiency using a constant local flux and a global solution. Kavanaugh [12] used the two-dimensional finite difference to test a borehole with concentric tubes. Lei [13] used a double two-dimensional cylindrical coordinate system to simulate a U-shaped ground heat exchanger. Zeng et al. [14, 15] used a different method for the finite line-source model. They measured ground temperature changes using a general method and an analytical equation derived from a point source solution instead of a finite difference. Many methods have improved computational and analytical tools for researching geothermal heat exchangers. 3D models are needed to understand ground heat exchangers (GHEs). Yoon and Luo [16], [17], Lee, Marcottea, Bouhacin [18]–[20], Fan [21], and Li [22] have used numerical models to simulate GHE components like layered ground profiles, vertical heat transfer inside and outside the GHE, dynamic temperature changes, groundwater advection, and thermal shortcircuiting between legs. Yang et al. [23] used constant and transient heat transfer methods to study the heat transfer parameters of a cylindrical source with fluctuating heat fluxes and simulate heat transfer with the soil surrounding the Ground Heat Exchanger (GHE), taking soil liquefaction into account. Li and Zheng [24] created a GHE field cross-section mesh using Delaunay triangulation. They created a vertical GHE-specific 3D unstructured finitevolume model. They investigated how fluid temperature changes at different depths affected the thermal process using vertical soil stratification. Kaltreider et al. [25] employed a transient finite-volume numerical model designed for thermoactivated foundation modeling to determine the appropriate grid style and size for CPU time estimation. This model was used to test and evaluate grid layouts during an experimental study. Gustafsson et al. [26] employed a 3D steady-state CFD model to analyze a U-shaped tube layout in a Scandinavian groundwater-filled GHE.

The Boussinesq approximation simulates free convective flow with density and temperature gradients. The modeling showed that natural convection greatly reduced the borehole's heat

resistance. Rees and He [27] studied fluid flow processes using a finite-volume numerical technique with a multi-block mesh to represent each GHE section in three dimensions. The experiments confirmed the model's fluid motion and diffusion predictions. The long-term study found heat transport at high circulation velocities at mean fluid and borehole wall temperatures. Low circulation velocities revealed temperature and heat-flux nonlinearities across the velocity range. The model examined the thermo-active foundation's three design parameters and annual construction simulations. Yang and Li [28] used analytical and numerical models to study borehole heat exchangers' short-term heat transmission. Their models were tested against real-world observations. Lee [29] included grout thermal capacitance and U-shaped tube fluid circulation in a three-dimensional borehole heat exchanger numerical model for fast time-step evaluations. Maestre et al. [30] simulated ground heat transport using a thermal resistance-capacity model. Borehole discretization and g-function integration The U-leg tube's thermal interference was ignored. Minaei and Maerefat [31] proposed a simpler thermal resistance capacity model for borehole heat exchanger thermal prediction. Their methodology worked well for time increments over an hour. A third study modeled heat transmission in borehole heat exchangers for a short time.

Ahmed [32] presented a GHE-efficient oval U-shaped tube borehole heat exchanger. ANSYS FLUENT unsteady state multi-physics CFD simulations examined this system's thermohydraulic performance in three dimensions. Zhu [33] used a validated heat transfer model to evaluate the transient thermal behavior of a vertical double U-shaped tube borehole heat exchanger. Inflow velocity, temperature, and operation interval were examined for radial and axial soil temperature distributions. Kerme [34] solved energy balance heat transport equations using an unsteady heat transfer approach and an implicit numerical technique to assess heat transmission inside and outside the borehole.

VGCHEs have been studied. Unfortunately, many of these calculations assume quasi-steady state heat transfer in the heat carrier fluid and back-fill material, even though the borehole wall, grout, and fluid all vary in temperature with time and depth. VGCHEs perform steadily even while soil surface temperature, solar radiation, wind speed, and sky radiation vary. Seasonal topsoil temperature fluctuations have not been explored in connection to fluid flow rates via the U-shaped tube ground-coupled heat exchanger. Due to the heterogeneity of soil surface conditions, VGCHE transient state performance has not been fully analyzed. This research creates a thorough 3D numerical model that accounts for ambient air temperature variations and a variety of soil surface conditions to fill in these gaps. This study examines the VGCHE's performance under dry sunlight, dry shelter, wet sunlight, and wet shelter soil surface conditions. Real-world data validates the model.

2. Numerical Model

2.1. **Model description:** The study focuses on investigating the performance of Vertical Ground Coupled Heat Exchangers (VGCHEs) under different soil surface conditions. Figure 1 provides a schematic diagram illustrating the experimental setup and components used for the study. The system consists of a vertical U-shaped tube heat exchanger, heat carrier fluid (water), tube, and the surrounding soil. The geometry and dimensions of the VGCHE, which are incorporated into the proposed model, are depicted in Figure 2(a) and (b). The U-shaped tube is buried at a depth of 17 m, with the surrounding soil extending to a depth of 20 meters. The U-shaped tube has a diameter of 0.0254 m and a thickness of 2 mm, while the distance separating the legs of the U-shaped tube is 0.0762 m (3 inches). For the radial boundary size of the model, a soil domain with a diameter of three meters is selected to represent an undisturbed

ISSN 2063-5346

soil boundary. The borehole is backfilled with the same soil that was excavated during drilling, as the subsurface soil mainly consists of red soil.

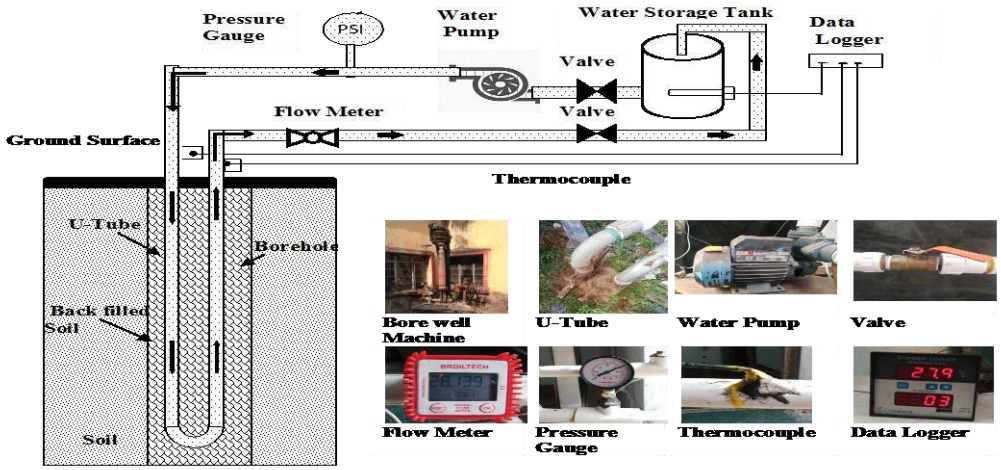

Figure 1. A Schematic diagram of vertical U-shaped tube ground coupled heat exchanger

A simulation model integrates thermal conduction and water advection to simulate the heat and mass transfer interactions between the U-shaped tube legs, soil, and water flow. The resulting model is a three-dimensional CFD simulation regulated by the convection-diffusion equation for temperature. In order to describe the heat movement within the Vertical Ground Coupled Heat Exchanger, the governing equations are solved using the Finite Volume Method (FVM) (VGCHE). These factors consist of convective heat transfer from the fluid within the inner U-shaped tube wall, conduction from the tube tube to the soil, conduction from the soil to the soil, convection from the environment at the top of the soil, and convection from the soil and the environment around the borehole.

The material properties of U-shaped tube, including its physical characteristics, as well as the mean values for these properties, are mentioned in Table 1. The Fluent software's material database is utilized to obtain the properties of water.

Table 1. Material properties required for proposed model

Material	**Density ρ (kg/m^3)**	**Specific Heat C_p(J/kg K)**	**Thermal Conductivity k(W/m K)**
U-Shaped Tube (GI)	8030	502.48	16.27
Water	999.6	4188	0.6

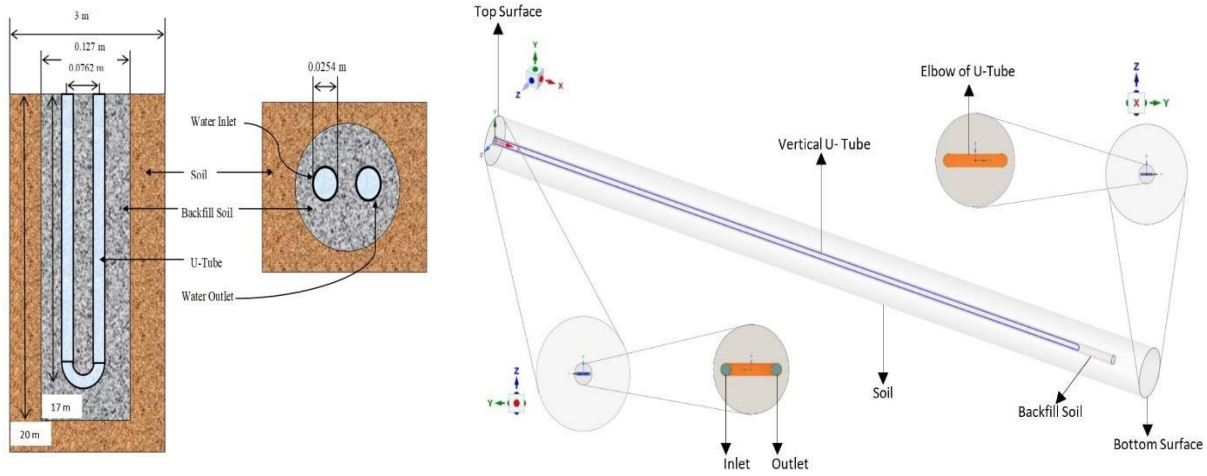

(a) (b)

Figure 2. (a) Proposed model system dimensions, (b) 3-D CFD proposed model of U-shaped Tube

The 3D transient heat transfer model that was used contains a number of assumptions. First, it disregards the effects of temperature changes on the water, U-shaped tube, and soil, assuming their properties will remain constant. Additionally, the subterranean soil is considered homogeneous and free of subsurface water movement.

2.2 Meshing: Three-dimensional modelling and mesh creation were accomplished with the help of ANSYS Workbench, while thermal analysis was simulated with Fluent. Tetrahedral meshes in Ansys 19.0 fluent were used to mimic the physical model, as seen in Figure 2. The mesh was refined around and inside the tube to produce accurate results, though the mesh was lowered away from the U-shaped tube to bring the total mesh count down. There were 35,947,388 meshes in total. The grid independence test was used to establish the range of meshing sizes.

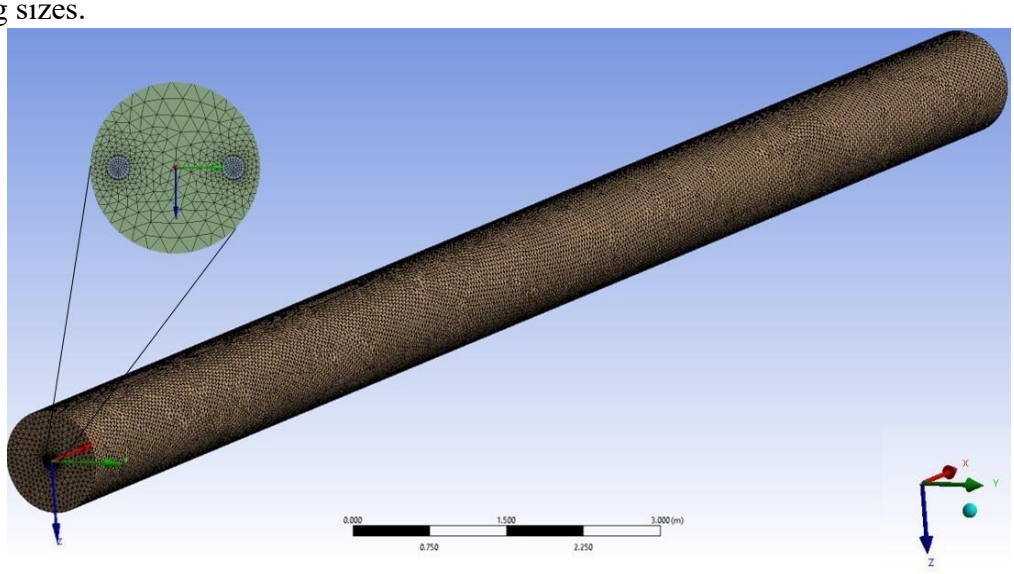

Figure2. Meshing of VGCHE

2.3 Grid Sensitivity Test: Ensuring the numerical solution's relevance and accuracy, as well as minimizing errors and computation time, requires the simulation to be gridindependent. A transient grid independence test, as depicted in Figure 3, was performed to certify convergence of the results. Researchers evaluated the outlet temperature at 6, 9, and 12 hours into the

simulation to see how the mesh element number affected the heat transfer. The maximum error for the first three mesh models of meshing element number 810280, 1100050 and 1820090 was found to be 0.87 K, 1.265 K, and 0.91 K for simulation time 6h, 9h, and 12 h respectively, while the maximum error for the next three mesh models of mesh element number 2860000, 3594738, and 3960000 was only 0.03 K, with a corresponding relative error of 0.09%. As the mesh element number increased, the computation time also increased significantly. As a result, the mesh model with an order of 3594738 was selected for simulation due to its accuracy and computational efficiency.

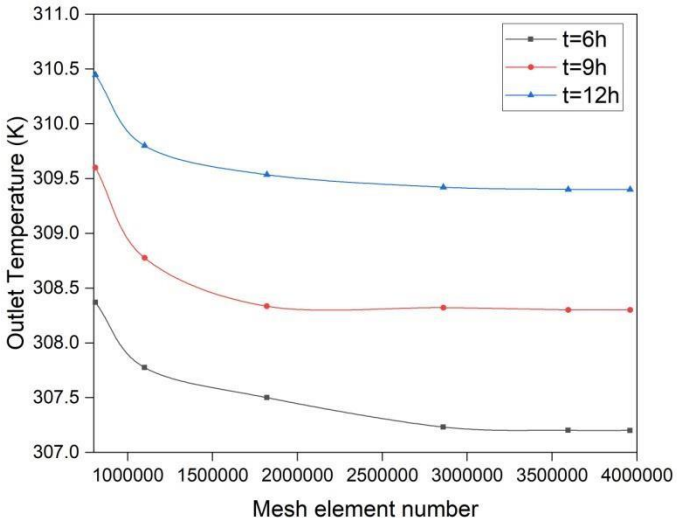

Figure 3. Transient Grid sensitivity test

2.4 Solution Methodology: A simple numerical approach with second-order implicit transient formulation was used to simulate the flow field, temperature field, pressure field, and coupled heat transfer process between the fluid and the surrounding soil. The unsteady simulations were carried out using the ANSYS FLUENT 19.0 program. The convergence was considered attained when the residuals for the continuity, momentum, and energy equations were less than 10-3 and 10-6, respectively. Simultaneously, the momentum equation for the fluid and the energy equations for the fluid, U-shaped tube, backfill soil, and surrounding soil were solved. As the turbulence model, the conventional k–ε model was used. The simulation was run for 24 hours with a time step of 60 seconds. During this time, the solver's calculation activities were used to track the area-averaged inlet and output flow, borehole wall temperatures, and pressure every hour.

2.5 Boundary conditions: A user-defined function (UDF) in the 3D transient heat transfer model determines the initial temperature of the soil and backfill. The bottom surface has a Dirichlet boundary condition, whereas the soil-side radial far surface is adiabatic. To account for heat exchange between the U-shaped tube and the soil, the Neumann boundary condition is applied at the contact boundary. A velocity inlet is set at the inlet boundary with a constant temperature of 288.15 K for heating mode and 311.15 K for cooling mode, as well as flow velocities of 0.12, 0.3, and 0.5 m/s. A pressure outlet is used to define the outlet boundary condition. Temperature fluctuations on and below the soil surface vary depending on soil surface conditions such as dry sunlight, dry sheltered, wet sunlight, and wet sheltered. To account for these factors, a convective boundary condition is applied to the upper surface, with

ISSN 2063-5346

the effective temperature calculated using measured air temperature, wind speed, and solar radiation data.

2.6 Governing equations: In order to analyse the dynamic properties of heat transfer and flow of fluids within solid and fluid regions, it is essential to solve the equations of "conservation of mass, momentum, and energy in a three-dimensional and unsteady state. These equations can be represented as follows" [40]:

2.6.1 Conservation of mass

$$\frac{\partial \rho}{\partial t} + \nabla.(\rho \vec{v}) = 0 \tag{1}$$

2.6.2 Momentum equation:

$$\frac{\partial}{\partial t}(\rho \vec{v}) + \nabla.(\rho \vec{v}\vec{v}) = -\nabla p + \nabla.\bar{\bar{\tau}} + \rho \vec{g} + \vec{F} \tag{2}$$

2.6.3 Energy Equation: In the solid domain, heat conduction is represented by the following energy conservation equation.

$$\frac{\partial}{\partial t}(\partial cT)dV = \lambda.\left(\frac{\partial T}{\partial X} + \frac{\partial T}{\partial Y} + \frac{\partial T}{\partial Z}\right).dA \tag{3}$$

A fluid's convection-conductive heat transfer can be described by the energy equation shown in Eq.

$$\frac{\partial(\rho\varphi)}{\partial t}dV + \mathrm{div}(\rho\varphi u)dV = (\Gamma.\mathrm{grad}\varphi)dV + S_{\varphi}dV \tag{4}$$

where, $\partial(\rho\varphi)/\partial t$, represents the change in $\rho\varphi$ with respect to time; the convective term, $\mathrm{div}(\rho\varphi u)$, represents the transport of $\rho\varphi$ by the fluid flow u, $\Gamma.\mathrm{grad}\varphi$, represents the diffusion of $\rho\varphi$ due to gradients in φ, and S_{φ} represents any additional sources of $\rho\varphi$ within the system.

The realizable κ-ε turbulence model is used to simulate turbulent energy dissipation near the tube wall within the boundary layer. This model is well-known for accurately capturing flows with boundary layers subject to strong adverse pressure gradients, separation, and recirculation. It ensures fast and precise convergence, making it ideal for high Reynolds number applications.

$$\frac{\partial(\rho k)}{\partial t} + \mathrm{div}(\rho k\vec{v}) = \mathrm{div}\left[\frac{\mu_t}{\sigma_k}\mathrm{grad}k\right] + 2\mu_t {S_k}^2 - \rho\varepsilon \tag{5}$$

$$\frac{\partial(\rho\varepsilon)}{\partial t} + \mathrm{div}(\rho\varepsilon\vec{v}) = \mathrm{div}\left[\frac{\mu_t}{\sigma_\varepsilon}\mathrm{grad}\varepsilon\right] + C_{1\varepsilon}\frac{\varepsilon}{k}2\mu_t {S_k}^2 - C_{2\varepsilon}\rho\frac{\varepsilon^2}{k} \tag{6}$$

$$\mu_t = \rho C_\mu \frac{k^2}{\varepsilon} \tag{7}$$

C_μ ,σ_ε, σ_k,$C_{1\varepsilon}$ and $C_{2\varepsilon}$ are the scientific parameters as follows:

$C_\mu = 0.09$, σ_ε=1.2, σ_k=1, $C_{1\varepsilon} = 1.44$, and $C_{2\varepsilon} = 1.9$

ISSN 2063-5346

2.6.4 Undistributed soil temperature equation: Analytical measurements of soil temperatures can be obtained for different soil surface conditions. The change in soil temperature T (y, t) can be represented using the transient heat conduction equation [8] in one dimension.

$$\frac{\partial^2 T(y,t)}{\partial y^2} = \frac{1}{\alpha}\frac{\partial T(y,t)}{\partial t} \quad (8)$$

Where α denotes soil thermal diffusivity and y denotes depth variation below the ground surface. A solution to the above equation can be found at the surface of the earth using the appropriate boundary condition equation.

$$-K\frac{\partial T}{\partial y}\Big|_{y=0} = CE - LR + SR - LE \quad (9)$$

Where, CE represents air-soil convective energy exchange, while thermal conductivity is represented by K, Long wave radiation, solar radiation, and latent heat flux by evaporation are represented by LR, SR, and LE.

The following expression can be derived from Equation (9) [35],

$$-k\frac{\partial T}{\partial y}\Big|_{y=0} = h_s\left(T_a - T|_{y=0}\right) - \varepsilon\Delta R + \alpha_0 S(t) - \dot{m}_e L \quad (10)$$

$$-k\frac{\partial T}{\partial y}\Big|_{y=0} = h_e\left(T_e - T|_{y=0}\right) \quad (11)$$ Here,

$$h_e = h_s(1 + 0.0168 f R_1) \quad (12)$$

$$T_e = \frac{1}{h_e}\left[h_s(1 + 0.0168 f R_1 \gamma)T_a + \alpha_0 S(t) - \varepsilon\Delta R - 0.0168 f R_2 h_s(1-\gamma)\right] \quad (13)$$

$$h = h_c + h_r \quad (14)$$

$$h = 2.8 + 3v_c \quad (15)$$

$$h = 4\varepsilon\sigma(T_a + 273.15)_{r\ 3} \quad (16)$$

Here α_0 is the surface soil radiation absorptivity, S(t) is Fourier-transformed solar radiation intensity, ΔR is the difference between the black substance's emitted radiation at the surrounding air temperature and the soil surface's emitted radiation exposed to the sky and surroundings, $\dot{m}_e$ denotes the rate of soil surface mass evaporation, ε refers to the ground surface's emittance, γ and f represent the relative humidity and moisture content of the soil, respectively.
R_1=103 Pa. K^{-1} and R_2=609 Pa are constants.

In general, the periodic function T_e is able to be represented as an annual and daily Fourier series.

ISSN 2063-5346

$$T_e = T_0 + \sum_{m=1}^{\infty} T_m \cos(m\omega t - \psi_m) \quad (17)$$

One-dimensional heat conduction equation solution: (with the assumption that T is finite for y→∞) is expressed as follows:

$$T(y,t) = t_0 + \sum_{m=1}^{\infty} t_m \exp[i(m\omega t) + \alpha_m y) \quad (18)$$

Here,

$$\alpha_m = -(1-i)(\omega\sigma cm/2k)^{1/2} \quad (19)$$

After replacing Te and T(y, t) with equations (17) and (18) respectively in equation (11), some algebraic manipulation can yield the following outcome.

$$T = T_0 + \sum B_m \exp(-m^{1/2}\alpha y)\cos(m\omega t - m^{1/2}\alpha y - \psi_m - \beta_m) \quad (20)$$

Here,

$$B_m = T_m \left[(1 + m^{1/2}\mu)^2 + m\mu^2\right]^{-1/2}_1 \quad (21)$$

$$\mu = \left(\frac{k\omega\sigma c}{2}\right)^{\bar{2}} / h_s \quad (22)$$

$$\beta_m = \tan^{-1}\left[\frac{m^{1/2}\mu}{(1+m^{1/2}\mu)}\right] \quad (23)$$

2.7 Soil undistributed temperature and Soil properties measurement: During Fourier analysis and CFD simulations, soil is typically considered to be homogeneous with constant physical properties. These properties are obtained by using a constant thermal analyser with an SH-1 probe, as illustrated in Figure 4(a). Measuring the undistributed temperature of the soil requires data on the radiation from the sun, the ambient temperature of the air, and the wind speed. As shown in Figure 4(b), the radiation from the sun, wind speed, and ambient air temperature were measured at the National Institute of Technology in Jamshedpur using a Radiation from the sun and Meteorological Parameter device. These data were recorded every minute throughout the year and are available online on the CWET website, which is managed by the Ministry of New and Renewable Energy (MNRE), Government of India. The ambient temperature of air data was represented in the form of a Fourier series, and the daily mean average temperature was calculated. In 2021, the highest daily mean average temperature was recorded on June 17 during the summer season, while the lowest daily mean average temperature was recorded on December 28 during the winter season.

ISSN 2063-5346

(a) (b)

Figure 4. (a) A thermal analyzer with an SH-1 probes for thermal conductivity and diffusivity tests, (b) Measurement of Meteorological Parameters at CWET station, NIT Jamshedpur

Table 2 and Table 3 present the physical properties of dry soil and soil with a water content of 20%, respectively. The soil underneath the surface is entirely saturated and primarily consists of red soil. The borehole is filled with original soil which is having water content of 20%.

Table 2. Dry soil Properties

S.no.	Parameter	Symbol	Value	Unit
1.	Thermal conductivity of Soil	K	0.5642	W/m K
2.	Density of soil	ρ	1968	Kg/m^3
3.	Specific heat capacity of soil	c_p	941.86	J/kg K

Table 3. Wet soil Properties (20% of water content)

S.no.	Parameter	Symbol	Value	Unit
1.	Thermal conductivity of Soil	K	1.19	W/m K
2.	Density of soil	ρ	2029.80	Kg/m^3
3.	Specific heat capacity of soil	c_p	756.108	J/kg K
4.	Soil surface absorptivity	α_0	0.65	-
5.	Emittance of earth surface	ε	0.8	-
6.	Relative humidity of soil	ϒ	0.04	-

3. Experimental Model: At the National Institute of Technology in Jamshedpur, India, a ground-coupled vertical U-shaped tube heat exchanger system has been established, comprising a water pump, control valve, data logger, thermocouple, digital flow meter, pressure gauge, water tank, and W1209 digital temperature controller thermostat module. The system's schematic diagram (Figure 1) displays a close loop vertical U-shaped tube. The installation process involved drilling a 20m (65.6-foot) vertical borehole with a 0.127m (5inch) diameter using a boring machine, after which a U-shaped tube made of GI tube with a diameter of 0.0254m (1 inch) and a thickness of 0.002m was inserted into the borehole to a depth of 17m. The legs of the U-shaped tube were spaced 0.0762m (3 inch) apart and were in direct contact

with the soil. The U-shaped tube's inlet was linked to a single-phase water pump with a pumping power of 0.37 kW (0.5 HP) and a discharge capacity of 2,050 LPH. The inlet and outlet of the U-shaped tube were linked to a PVC tube with a diameter of 0.0254m (1 inch) and a wall thickness of 0.001m. When above the ground surface, the PVC tubes were insulated with glass wool to minimize heat transfer losses. The water pump circulated water inside the U-shaped tube, and the outlet was connected to a water storage tank. The temperature in the water tank was controlled using a W1209 digital temperature controller thermostat module with a measuring accuracy of 0.1 ºC.

The temperature and flow rate of the fluid going in and coming out must be continuously monitored in order to make sure the ground-coupled heat exchanger system operates smoothly and efficiently. RTD-100 sensors and thermocouples with a 0.1°C accuracy are used to measure temperature. With 1% precision, a digital flow meter is used to measure the fluid's flow rate. These instruments are essential for system performance analysis. Throughout the testing process, parameters such as intake temperature, output temperature, water flow discharge rate, and flow pressure were monitored to characterize the system's performance. The borehole was backfilled with red soil that had a water content of 20%, and the subterranean earth at the site was saturated. During the experimental test, the fluid's inlet temperature was continuously monitored and recorded, and the data was plotted as a graph to observe its behaviour over time. The inlet temperature for the simulation is the average temperature of the fluid entering every hour. The simulation was carried out using a fluid velocity of 0.12 m/s, which corresponded to the real experiment velocity. All additional parameters pertaining to the experimental system's boundaries and initial circumstances remained constant throughout the simulation.

3.1 Model validation: The comparison of the outlet temperature of the water flowing through the U-shaped tube in the CFD simulation and the experimental data is shown in Figure 5. The graph shows that the patterns of temperature changes near the outlet remained similar in the simulated and experimental data. The temperature readings obtained from the simulation and the experiment only differed by a maximum of 0.4 K (1.28%). It is essential to point out that the inlet temperature was the same for the simulation and the experiment.

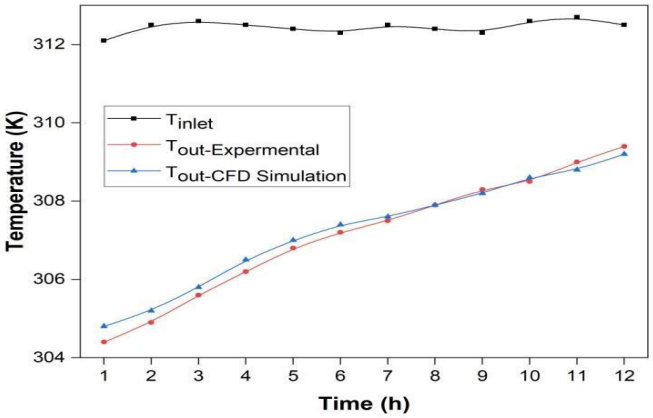

Figure 5. Validation of CFD simulation with experimental result

4. Results and discussions

This section is devoted for analysis of 3D numerical model that considers the transient behaviour of surrounding ambient air temperature fluctuations and various soil surface conditions. The effect of velocity variation on VGCHE performance due to different soil surface conditions has been analysed.

4.1.Soil temperature measurement

At the Jamshedpur location in India, the soil temperature distribution is affected by the atmospheric temperature and solar radiation. To simulate this variation, a six-term Fourier series equation (as shown in Table 4 and 5) with user-defined parameters is used. The equation incorporates the atmospheric temperature (T_e) and heat transfer coefficient (h_e) to model soil temperature fluctuations for all four soil surface conditions. The soil temperature varies periodically with depth up to 4 meters annually. The variation in soil temperature with time is applied using a user-defined function (UDF) for the hottest and coldest days of various soil surface conditions.

Table 4. Fourier coefficients for the measurement of ambient temperature at Jamshedpur

		$(T_a)_0$	$(T_a)_1$	$(T_a)_2$	$(T_a)_3$	$(T_a)_4$	$(T_a)_5$	$(T_a)_6$
Annual	Fundamental term	26.33						
	Coefficient of cosine term		-4.84	-2.39	-0.44	-0.46	0.45	-0.50
	Coefficient of sine term		0.32	-0.93	0.30	-0.83	-0.16	-0.13
Hottest summer day	Fundamental term	36.55						
	Coefficient of cosine term		-3.17	-0.33	-0.28	-0.04	0.27	-0.04
	Coefficient of sine term		-4.69	0.72	0.03	-0.10	-0.21	-0.16
coldest	Fundamental term	19.5						
	Coefficient of cosine term		-1.69	0.34	-0.31	0.18	-0.04	-0.04
	Coefficient of sine term		-2.39	0.27	-0.29	-0.29	-0.04	-0.19

Table 5. Fourier coefficients for the measured solar radiation at Jamshedpur

		S_0	S_1	S_2	S_3	S_4	S_5	S_6
Annual	Fundamental term	188.5						
	Coefficient of cosine term		-22.73	-32.48	3.187	-11.47	10.05	-6.60
	Coefficient of sine term		26.67	-5.584	11.27	1.353	2.948	3.623
Hottest summer day	Fundamental term	242.2						
	Coefficient of cosine term		-384.6	181.6	-33.36	-15.73	22.87	-21.19
	Coefficient of sine term		-19.31	15.64	-6.04	8.629	-7.86	-6.35
Coldest winter day	Fundamental term	156.7						
	Coefficient of cosine term		-265.8	155	-48.21	-8.655	17.17	-6.444
	Coefficient of sine term		-24.95	27.76	-10	-7.665	10.3	-2.285

The measured data of ambient air temperature and solar radiation is well represented with the Fourier coefficients as given in the Table 4 and Table 5. These coefficients are specified for the warmest and coolest days of the year. The measured data of temperature of air and radiation from sun for the hottest and coldest days of the year were used to determine the best curve fit

ISSN 2063-5346

for computing these values. Using these coefficients, the soil temperature is predicted for various soil conditions which are represented in Figure 8. Radiation from sun fluctuation and temperature fluctuation at Jamshedpur for hottest summer day (17th June 2021), coldest winter day (28th December 2021) and yearly is taken as six-term harmonica. The offered six harmonics are enough for capturing all of the measured data with an R^2 of close to 98%. A direct sunlight-exposed surface is sunlight surface and sheltered surfaces that don't receive direct sunlight. Effective temperature (T_e) of hottest summer and coldest winter day for different soil conditions are presented in Figure 7. The highest effective temperature is achieved near 03:00 PM and lowest effective temperature is achieved near 6AM for all soil surface conditions.

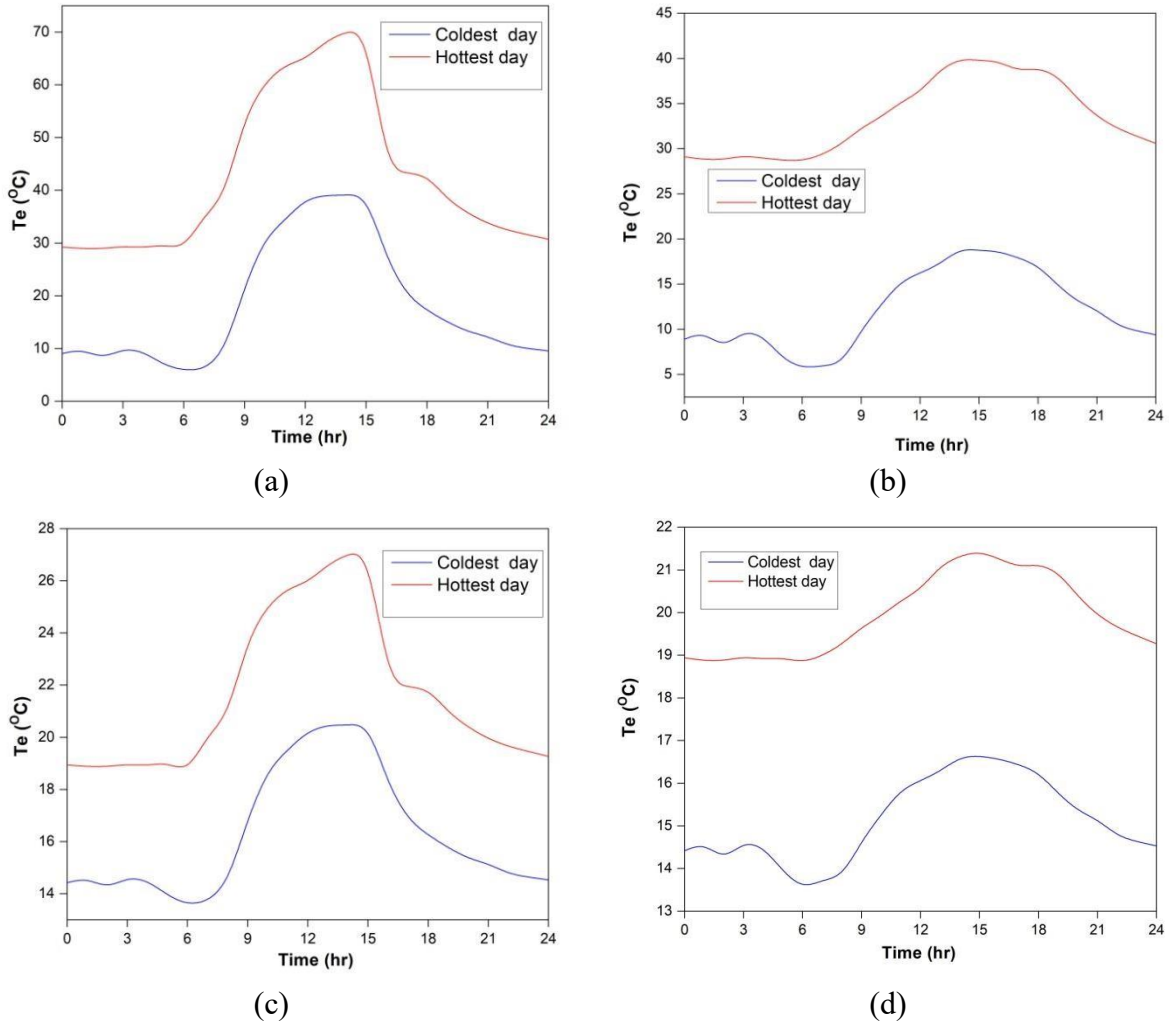

Figure 7. Hottest summer and Coldest winter day T_e fluctuation for (a) dry sunlight surface, (b) dry sheltered surface, (c) wet sunlight surface, and (d) wet sheltered surface

Table 6, table 7, and table 8 shows the coefficient of Fourier series for hottest summer day, coldest winter day and yearly fluctuation of effective temperature of various soil surface condition.

Table 6. Fourier analysis of effective temperature (T_e) fluctuation for hottest summer day (17th June 2021) in Jamshedpur (India) for various surface conditions								
T_e	**m**	**0**	**1**	**2**	**3**	**4**	**5**	**6**

Dry sunlight surface	T_m	43.3729	19.214	6.9999	1.6174	0.7078	1.2987	0.9805
	ψ_m		0.2879	0.1930	0.1297	0.3372	0.4185	0.4448
Wet sunlight surface	T_m	21.7872	3.8192	1.3333	0.3183	0.1358	0.2596	0.1913
	ψ_m		0.3184	0.2117	0.1229	0.3091	0.4289	0.4675
Dry sheltered surface	T_m	33.7702	5.6644	0.7945	0.2828	0.1169	0.3535	0.4806
	ψ_m		0.9757	1.1424	0.1074	1.1750	0.6570	0.3613
Wet sheltered surface	T_m	19.9501	1.2668	0.1777	0.0632	0.0261	0.0790	0.0393
	ψ_m		0.9758	1.1424	0.1074	1.1749	0.6570	1.3121

Table 7. Fourier analysis of effective temperature (T_e) fluctuation for coldest winter day (28th December 2021) in Jamshedpur (India) for various surface conditions.

T_e	m	0	1	2	3	4	5	6
Dry sunlight surface	T_m	22.9330	12.6948	6.6336	2.3347	0.6191	0.7325	0.4186
	ψ_m		0.2702	0.2092	0.3029	1.3182	0.5120	0.7653
Wet sunlight surface	T_m	17.3253	2.5029	1.2818	0.4594	0.1264	0.1381	0.0857
	ψ_m		0.2942	0.2142	0.3164	1.3838	0.5067	0.8075
Dry sheltered surface	T_m	16.7202	2.9380	0.4414	0.4364	0.3505	0.0650	0.2047
	ψ_m		0.9554	0.6787	0.7577	1.0033	0.8652	1.3423
Wet sheltered surface	T_m	16.1368	0.6571	0.0987	0.0976	0.0784	0.0145	0.0457
	ψ_m		0.9554	0.6787	0.7577	1.0034	0.8652	1.3423

Table 8. Fourier study of annual effective temperature (T_e) change in Jamshedpur, India, under different surface conditions.

T_e	m	0	1	2	3	4	5	6
Dry sunlight surface	T_m	28.8901	6.1044	3.8583	0.8184	1.2070	0.8557	0.7684
	ψ_m		0.2287	0.3037	1.1669	0.7017	0.0565	0.0223
Wet sunlight surface	T_m	19.0941	1.3231	0.8210	0.1716	0.2601	0.1788	0.1633
	ψ_m		0.2097	0.3106	1.1119	0.7433	0.0816	0.0050
Dry sheltered surface	T_m	23.5503	4.8570	2.5692	0.5424	0.9548	0.4849	0.5220
	ψ_m		0.0673	0.3714	0.5989	1.0596	0.3476	0.2449
Wet sheltered surface	T_m	17.6644	1.0863	0.5746	0.1213	0.2135	0.1084	0.1168
	ψ_m		0.0673	0.3714	0.5989	1.0587	0.3476	0.2449

Daily average effective temperature for the year 2021 for different soil conditions are presented in Figure 8. Soil receives highest radiation from sun and lowest evaporation in sunlight condition which in result highest temperature fluctuation. Lowest temperature fluctuation in wet sheltered condition due to lowest radiation from sun and highest evaporation. The dry sunlight soil condition has the highest amplitude fluctuation of temperature whereas the wet sheltered soil condition has lowest amplitude fluctuation of temperature.

ISSN 2063-5346

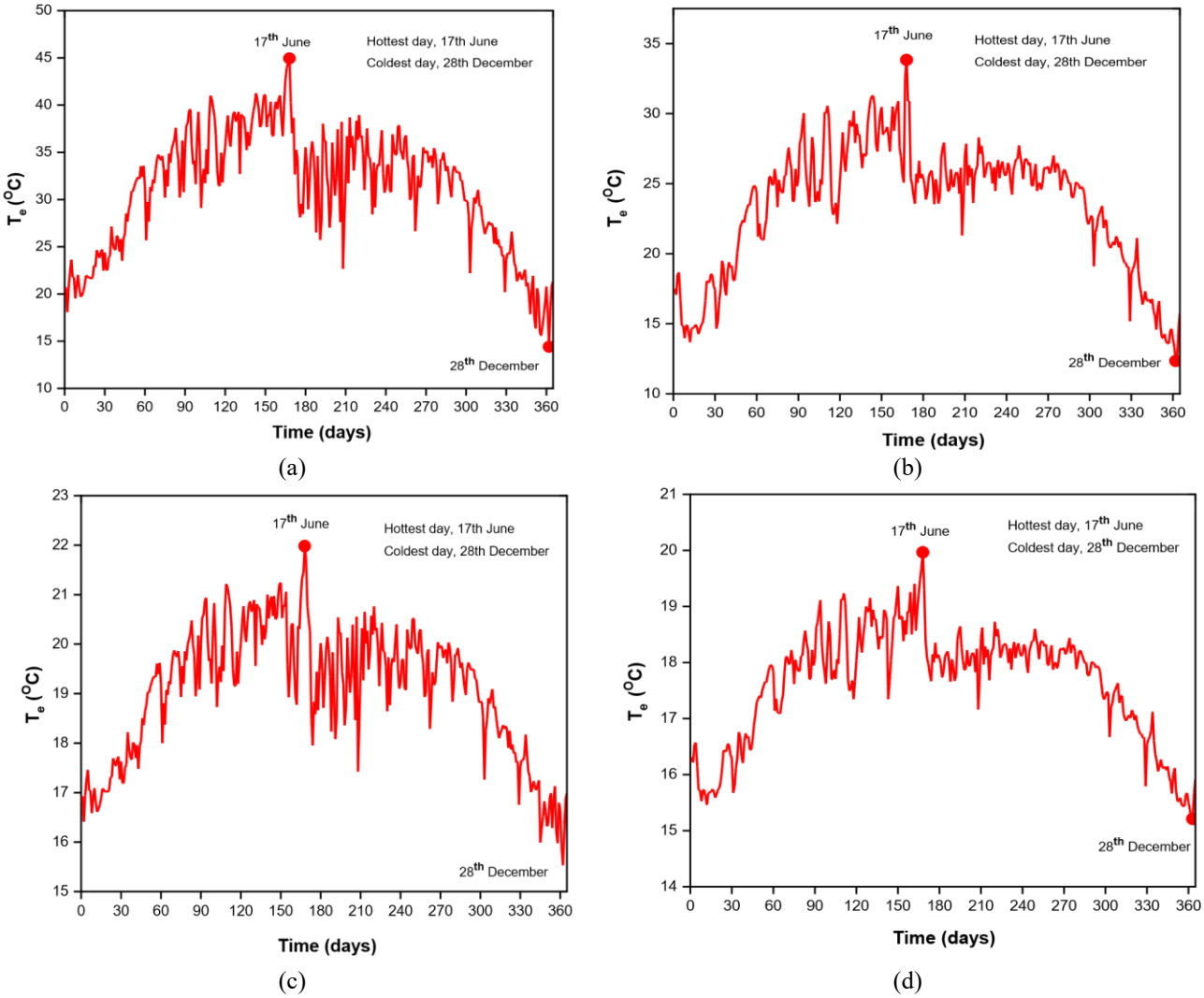

Figure 8. Daily T_e fluctuation for (a) Dry Sunlight (b) Dry Sheltered (c) Wet Sunlight (d) Wet Sheltered

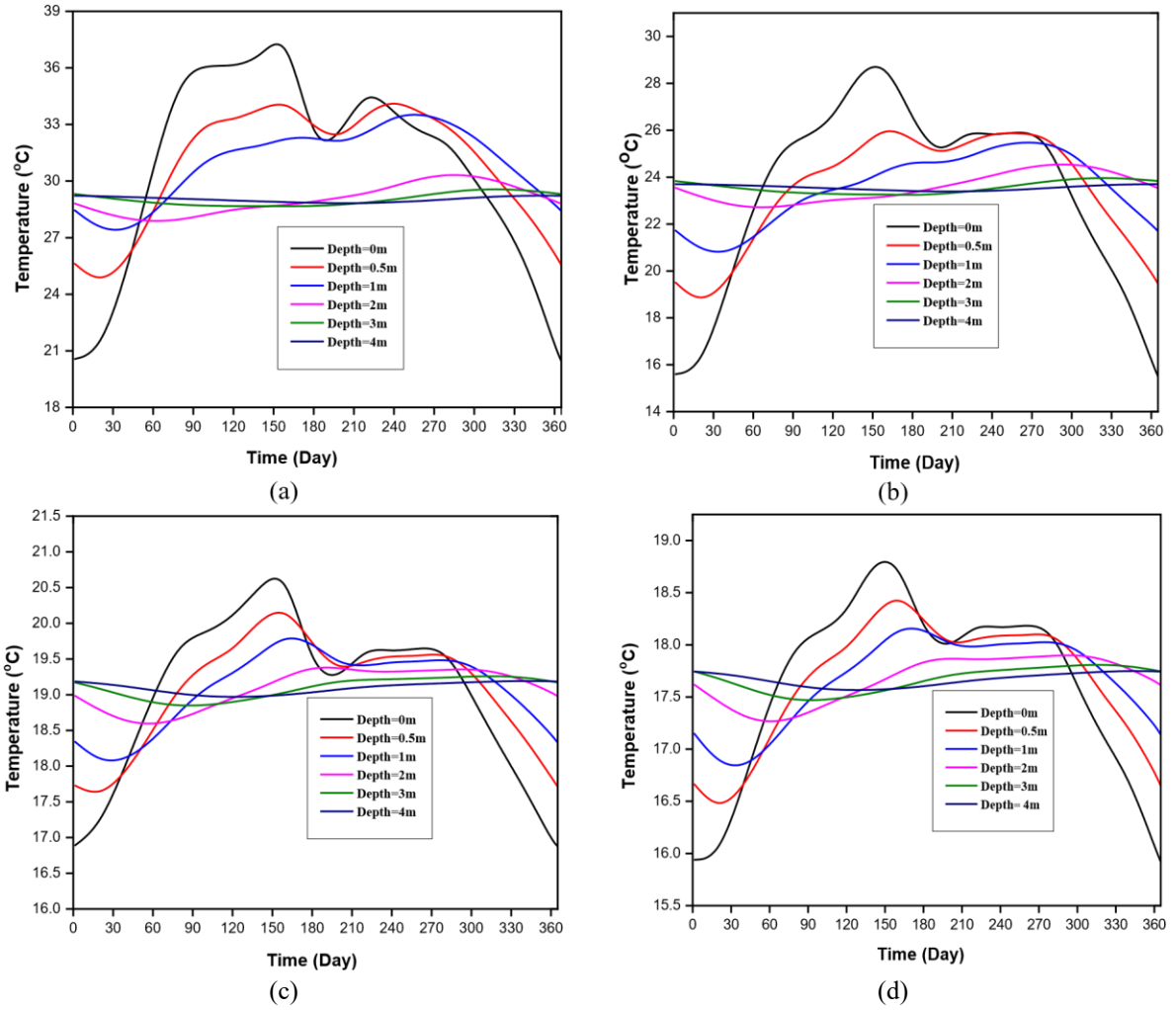

Figure 9. Yearly temperature Fluctuation in 2021, (a) Dry Sunlight, (b) Dry Sheltered, (c) Wet Sunlight, and (d) Wet Sheltered

Soil temperature fluctuation under various soil conditions throughout the year are depicted in Figure 9. The outcomes suggest that the temperature fluctuation at a depth of about 4m remains consistent which is termed as Undistributed soil temperature, shown in table 9. The predictions from the analytical model indicate that there is a substantial reduction of undistributed soil temperature with wet soil conditions which accounts for around 38.84% and 33.88% in sheltered conditions and sunlight condition respectively, whereas in dry sheltered soil conditions, it accounts a reduction of 18.45% in soil temperature in comparison with the dry sunlight condition. This indicates that the soil temperature is greatly influenced by the shade and moisture evaporation rate. Highest undistributed soil temperature is achieved for dry sunlight surface while wet sheltered surface achieved the lowest undistributed soil temperature among of other soil surface condition.

Table 9. Undistributed soil temperature for various soil surface conditions

Sr. No.	Soil surface condition	Undistributed soil temperature at depth below 4m.
1	Dry Sunlight	28.89 °C (302.04 K)
2	Dry Sheltered	23.56 °C (296.71 K)
3	Wet Sunlight	19.10 °C (292.25 K)
4	Wet Sheltered	17.67 °C (290.82 K)

Four different soil surface conditions are chosen to investigate the influence of VGCHE outlet temperature change. Soil properties for soil and back fill soil as Figure 1. are assumed of same properties for study the behaviour of different soil surface conditions. Like for dry soil surface condition, the soil and backfill soil properties will be same as of dry nature of soil. The hottest summer day and the coldest winter day are selected as two unfavourable situations. Simulation is run for 24 h, with time measured from 12 o'clock midnight. For hottest summer day water with velocity 0.12 m/s flowing with constant inlet temperature 311.15 K (38ºC) through U-shaped tube. Figure 10. Show the hottest day outlet temperature variation for coldest and hottest time with length for different soil surface conditions. During the coldest time lower outlet temperature is achieved as compared to hottest time of the day. Compared to the warmest time of the day, the temperature drops more during the coldest time. This is because the fluid flow is substantially slower than the heat diffusion capacity outside the U-shaped tube heat exchanger. The soil near the U-shaped tube will heat in radial direction and soil temperature will increase near the U-shaped tube. This resulted in the lower temperature drop during hottest time of the day. Minimum outlet temperate of VGCHE is achieved with wet sheltered surface Condition while dry sunlight condition achieved maximum outlet temperature. There is a substantial decrease of outlet temperature in wet sheltered conditions which accounts for 2.61 K and 2.25 K lower with respect to dry sunlight condition during coldest time and hottest time respectively. During summer season VGCHE works in cooling mode and lower outlet temperature is desired so wet sheltered condition most suitable among all other surface conditions.

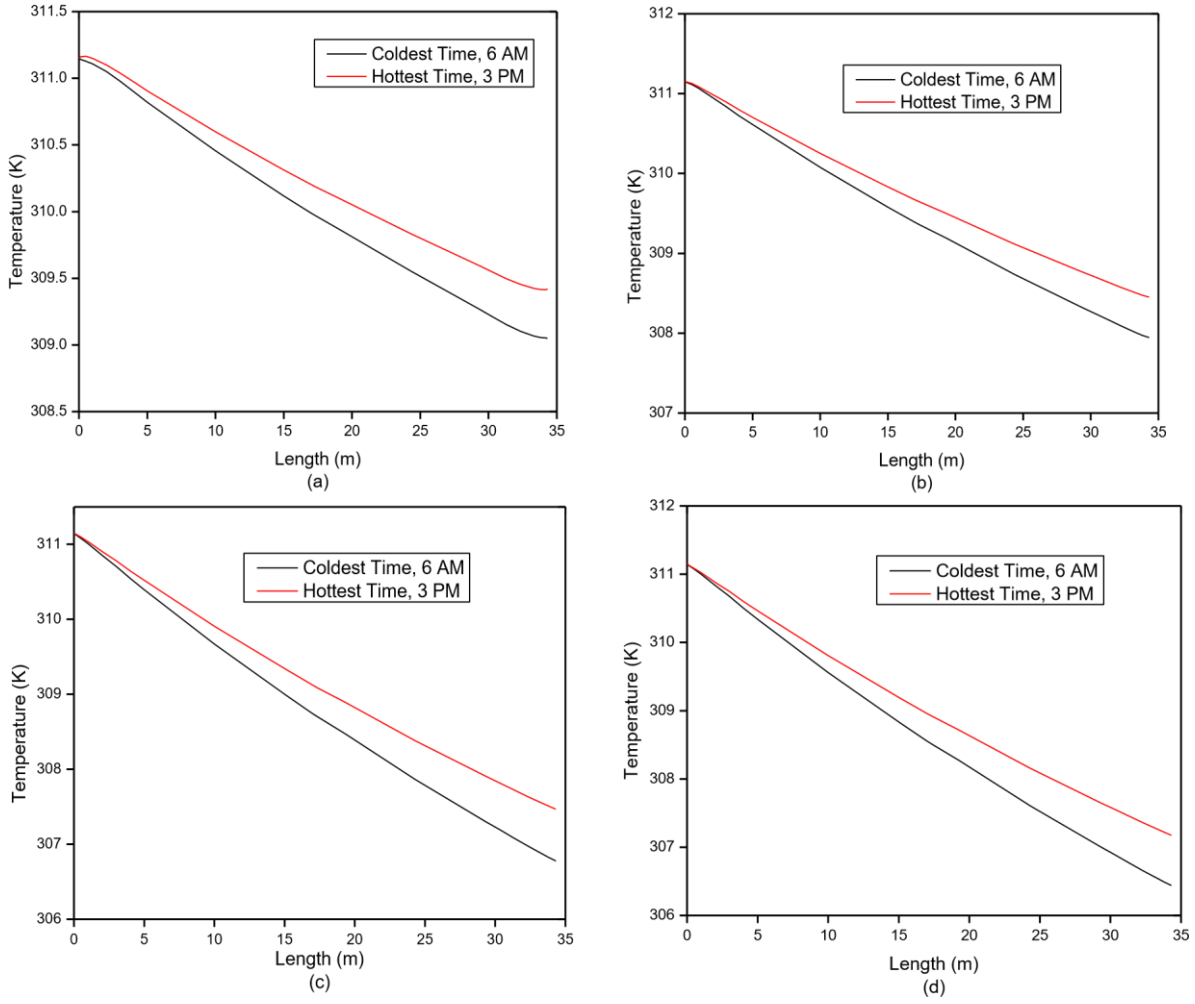

ISSN 2063-5346

Figure 10. Hottest day temperature variation for coldest time (6 AM) and hottest time (3 PM) with length for different soil surface conditions (a) Dry Sunlight (b) Dry Sheltered (c) Wet Sunlight and (d) Wet Sheltered, inlet temperature of 311.15 K (38ºC) at Constant Velocity of 0.12 m/s.

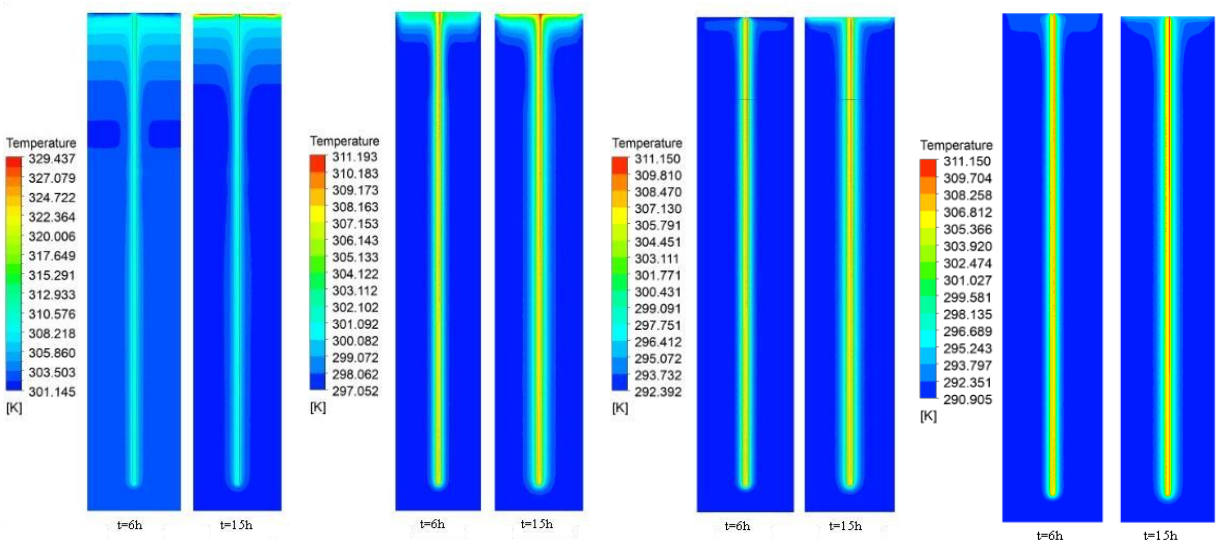

(a) (b) (c) (d)

Figure 11. Contour of Hottest day of temperature variation for coldest and hottest time for different soil surface conditions (a) Dry Sunlight (b) Dry Sheltered (c) Wet Sunlight and (d) Wet Sheltered, inlet temperature of 311.15 K (38^{oC}) at Constant Velocity of 0.12 m/s.

Temperature contour of hottest summer day is depicted in Figure 11. for coldest and hottest time of the day for various soil surface conditions. Near the leg of U-shaped tube there is rise in the soil temperature and rise in soil temperature is increasing as simulation time is increasing due to the heat charging by the water flow. The upper layer of soil temperature is varying due the surrounding air temperature and radiations falling on the surface. The variation due to surrounding is up to depth 4m.

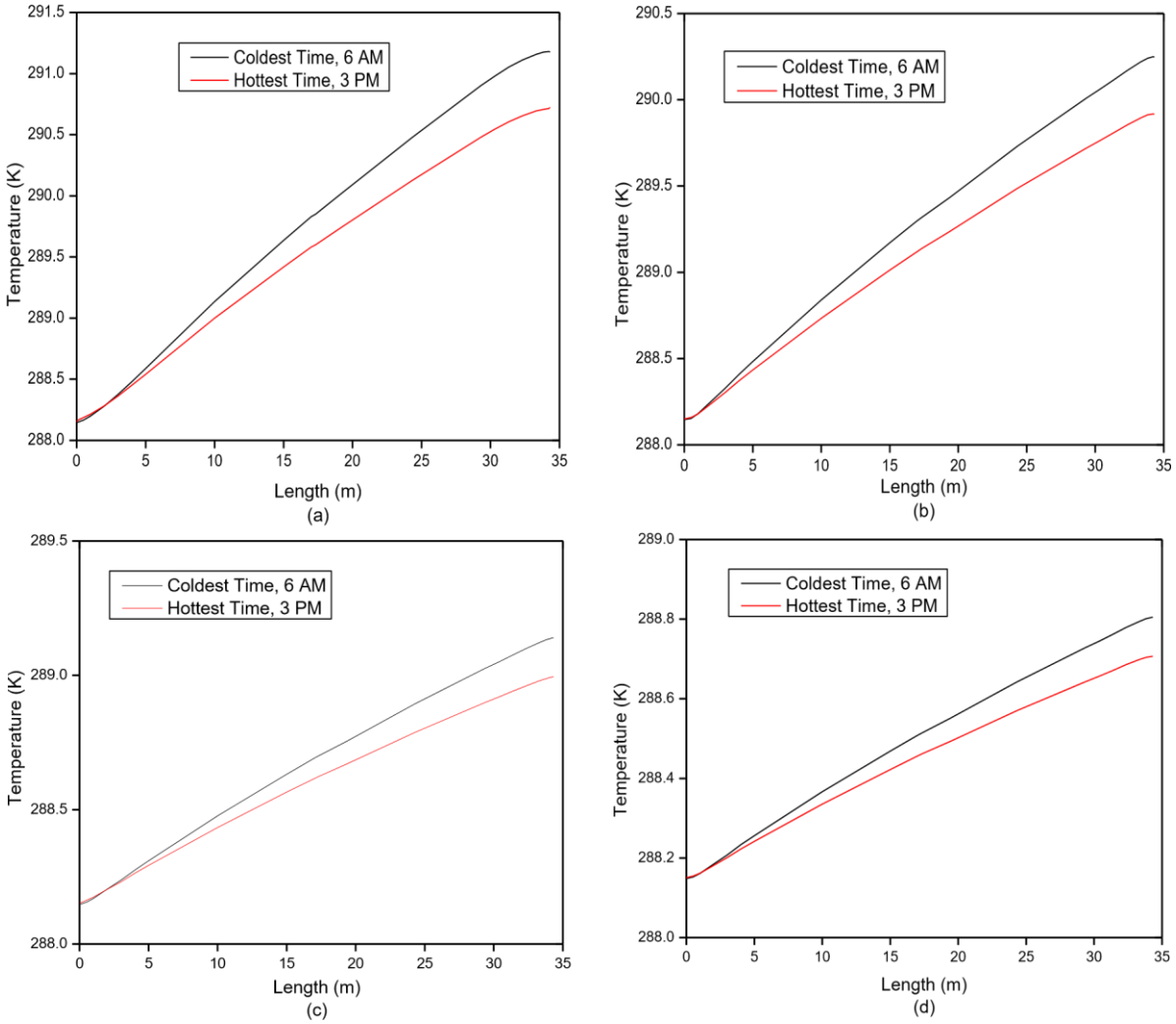

Figure 12. Coldest day temperature variation for coldest (6 AM) and hottest time (3 PM) with length for different soil surface conditions, (a) Dry Sunlight (b) Dry Sheltered (c) Wet Sunlight and (d) Wet Sheltered, inlet temperature of 288.15 K (15 ºC) at Constant Velocity of 0.12 m/s.

On the coldest winter day, water with a velocity of 0.12 m/s flowed through the U-shaped tube, maintaining a constant inlet temperature of 288.15 K (15°C). Figure 12 presents the variation in outlet temperature during the coldest and hottest times of the day for different soil surface conditions. During the coldest time, the outlet temperature was higher compared to the hottest time. This discrepancy can be attributed to the slower heat diffusion capacity outside the U-shaped tube heat exchanger in comparison to the convection heat transfer resulting from fluid flow. As time progresses, the soil near the U-shaped tube undergoes radial cooling, causing a decrease in soil temperature in its vicinity. Consequently, the temperature drop during the hottest time of the day is less significant, leading to reduced heat transfer in comparison to the coldest time. Among the different soil surface conditions, the maximum outlet temperature was achieved with a dry sunlight surface condition, while the minimum outlet temperature was obtained with a wet sheltered condition. Specifically, during the coldest time, the outlet temperature was 2.08 K higher in dry sunlight conditions compared to wet sheltered conditions, and during the hottest time, it was 1.73 K higher. During the winter season, when the ground-coupled heat exchanger operates in heating mode, higher outlet temperatures are desired.

ISSN 2063-5346

Therefore, a dry sunlight surface condition is considered the most suitable among all other surface conditions.

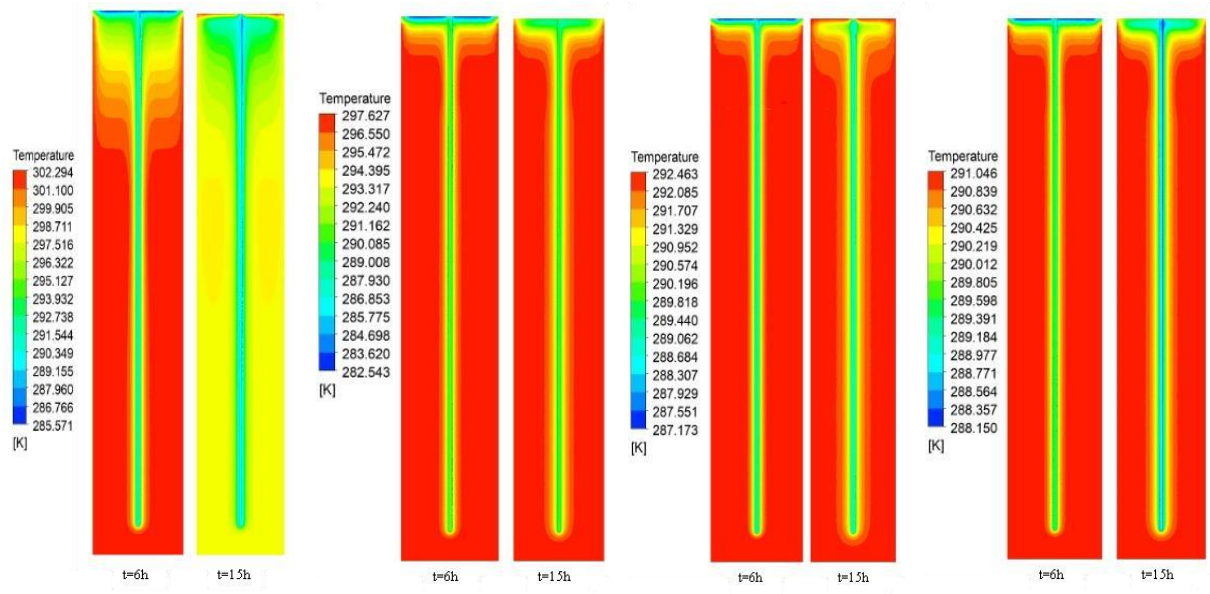

(a) (b) (c) (d)

Figure 13. Contour of Coldest day of temperature variation for coldest and hottest time with length for different soil surface conditions (a) Dry Sunlight (b) Dry Sheltered (c) Wet Sunlight and (d) Wet Sheltered, inlet temperature of 288.15 K (15 ºC) at Constant Velocity of 0.12 m/s.

Temperature contour of coldest winter day is depicted in Figure 13. for coldest and hottest time of the day for various soil surface conditions. Near the leg of U-shaped tube there is fall in the soil temperature and fall in soil temperature is increasing as simulation time is increasing due to the heat extraction by the water flow. For both hottest day and coldest day temperature contour the soil temperature variation is near the U-shaped tube up to radius of 0.5m.

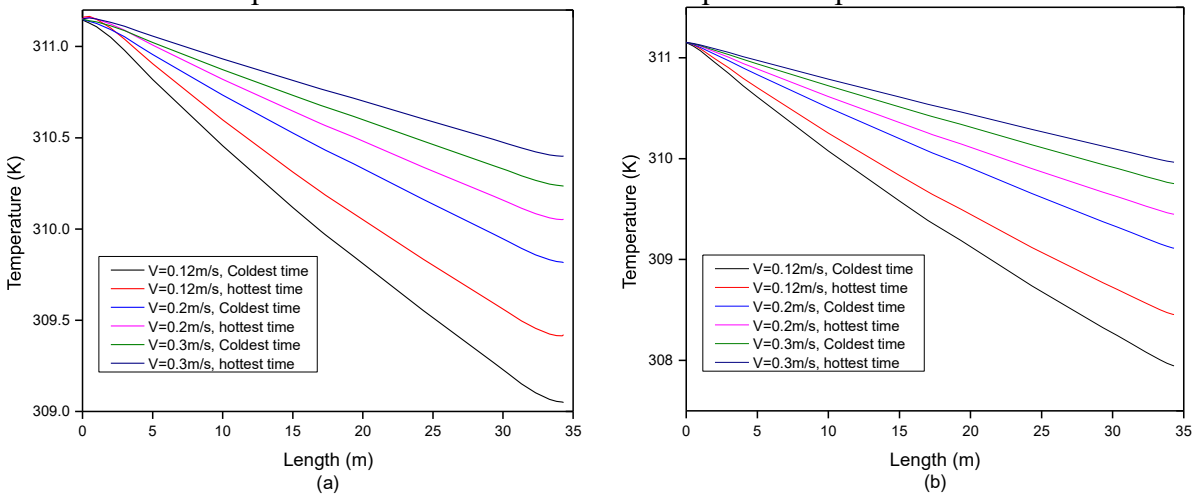

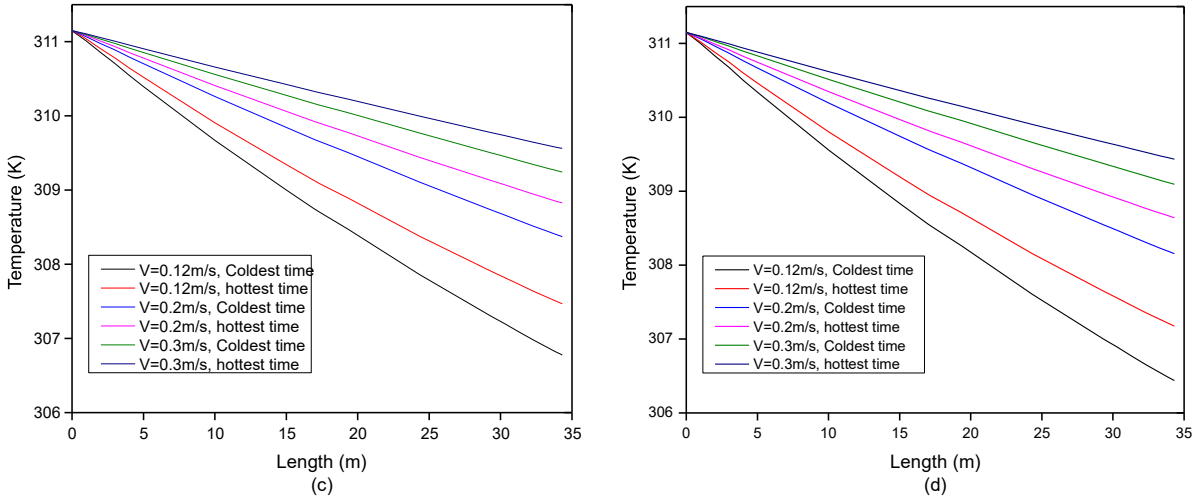

Figure 14. Hottest day temperature variation for coldest (6 AM) and hottest time (3 PM) with different velocity for (a) Dry Sunlight (b) Dry Sheltered (c) Wet Sunlight and (d) Wet Sheltered, inlet temperature of 311.15 K (38ºC).

The same simulation model was used to study outlet temperature variation at 0.2 and 0.3 m/s flow velocities. Figures 14 and 15 show outlet temperature variation for different soil surface conditions on the hottest summer and coldest winter days. On the hottest summer day, a lower flow rate caused a lower outlet temperature, while a higher flow rate increased it. On the coldest winter day, lower flow rates raised outlet temperatures, while higher flow rates lowered them.

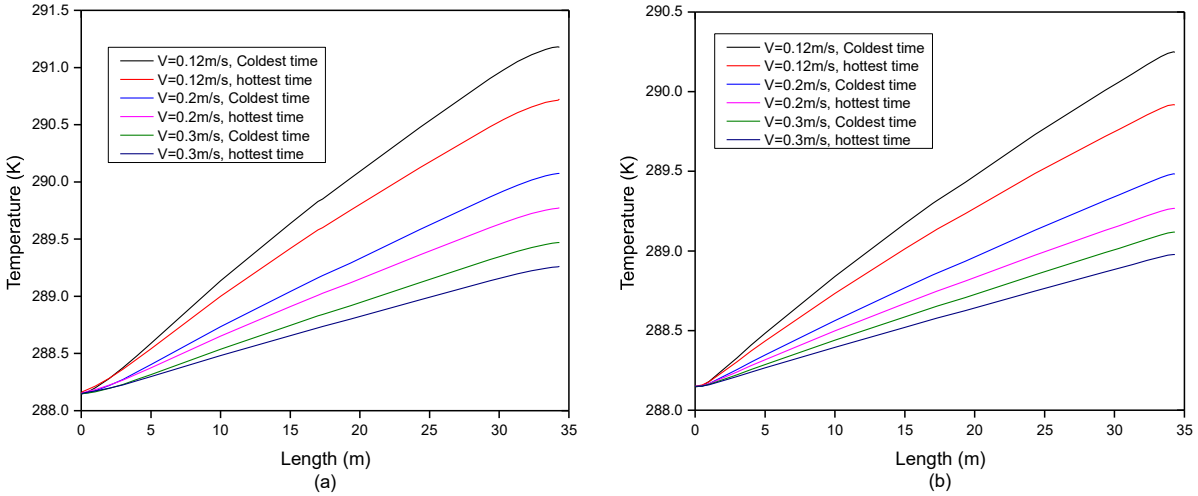

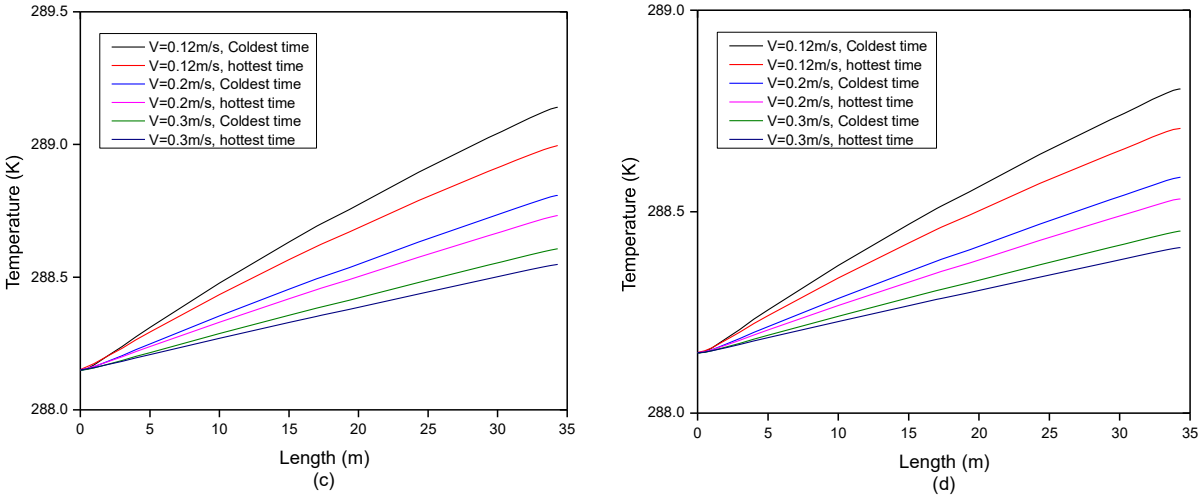

Figure 15. Coldest day temp variation for coldest (6 AM) and hottest time (3 PM) with different velocity of (a) Dry Sunlight (b) Dry Sheltered (c) Wet Sunlight and (d) Wet Sheltered, for inlet temperature of 288.15 K (15 ^{o}C)

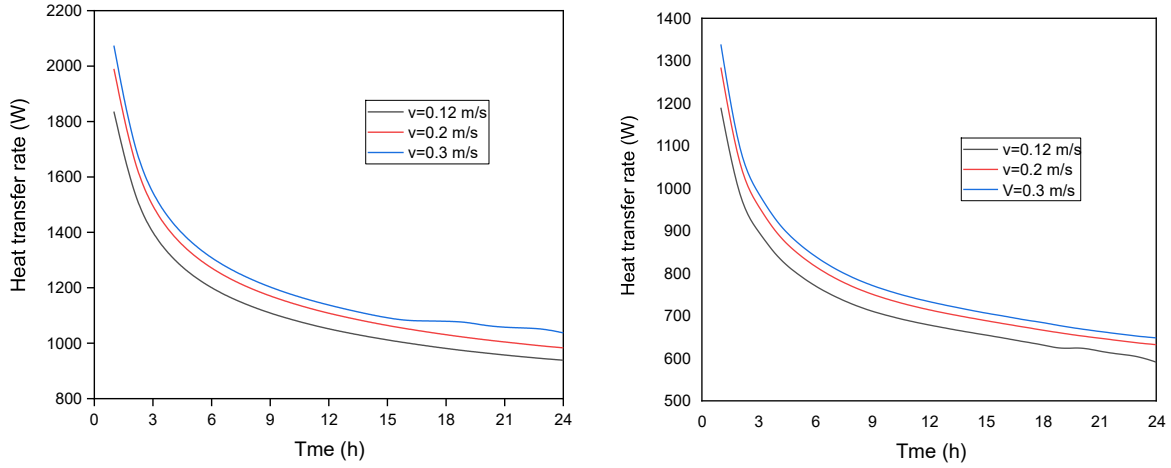

Figure 16. (a) Heat transfer rate for hottest day, wet sheltered condition under different flow velocity, (b) Heat transfer rate for coldest day, dry sunlit condition under different flow velocity

As illustrated in Figure 16, the heat transfer rate is shown for the hottest day (wet sheltered) and coldest day (dry sunlight) at flow velocities of 0.12, 0.2, and 0.3 m/s. During the heat charging phase, there was high heat transfer due to the temperature difference between the heat carrier fluid and the initial soil. The heat accumulated in the borehole because the heat diffusion outside the U-shaped tube heat exchanger was slower than the fluid flow. On the coldest winter day, heat was extracted from the surrounding soil, causing a decrease in its temperature. Conversely, on the hottest summer day, the soil temperature increased around the heat exchanger. The heat transfer rate reached a stable state after approximately 6 hours. Importantly, on the hottest summer day, increasing the flow velocity from 0.12 m/s to 0.2 m/s resulted in an 8.5% increase in heat transfer, and increasing it to 0.3 m/s resulted in a 13% increase. Similar trends were observed on the coldest winter day.

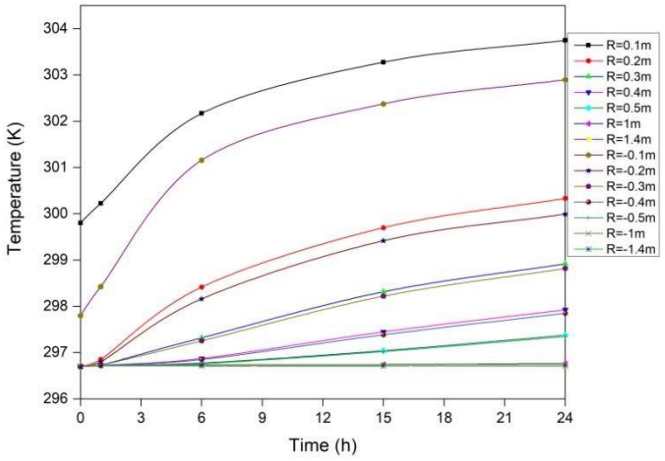

Figure 17. Variation of soil temperature with time at different radius from the axis at depth of 10m from soil surface

The radial temperature distribution within the soil under dry sheltered conditions was investigated using the same simulation model. Figure 17 illustrates the temporal variation of soil temperature at different radii, specifically at a depth of 10m from the soil surface, a flow velocity of 0.1m/s, and an inlet temperature of 311.15 K. The findings indicated that the soil temperature in proximity to the U-shaped tube experienced a rapid increase during the initial 5 hours. Significantly, the inlet side's soil temperature was greater than the outflow side's soil temperature close to the U-shaped tube's leg. Within the first hour of simulation, the soil temperature at a radius of 0.1 m rose by 3.3 K, followed by a sharp increase over the next 5 hours. Subsequently, there was a gradual temperature rise up to the 24-hour mark. In contrast, the temperature increase at a radius of 0.5 m was not evident until 6 hours, and it reached 0.5 K after a continuous heat charging period of 15 hours. In addition, there was little change in temperature during the course of the simulation at a radius of 1 m.

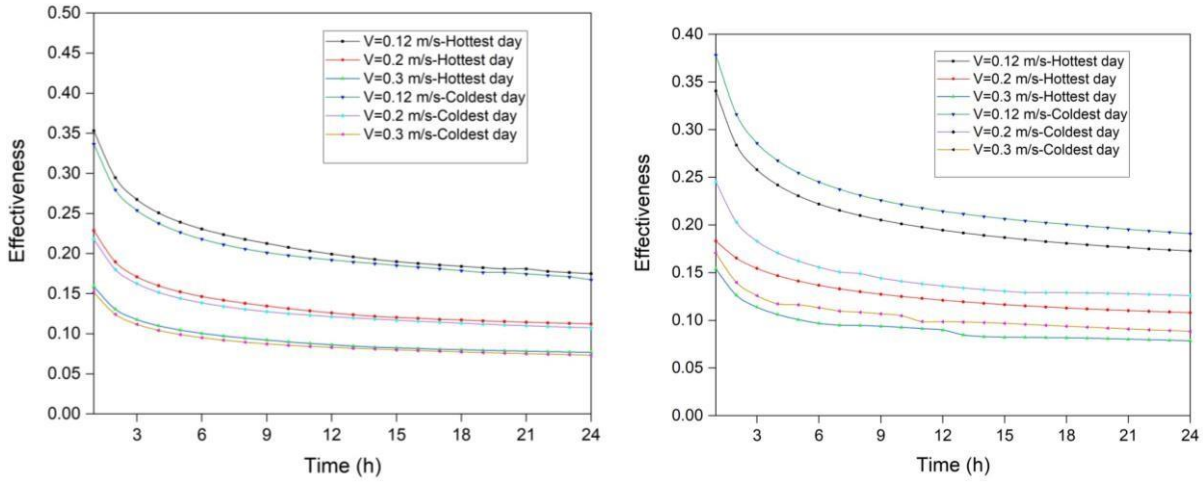

(a) (b)

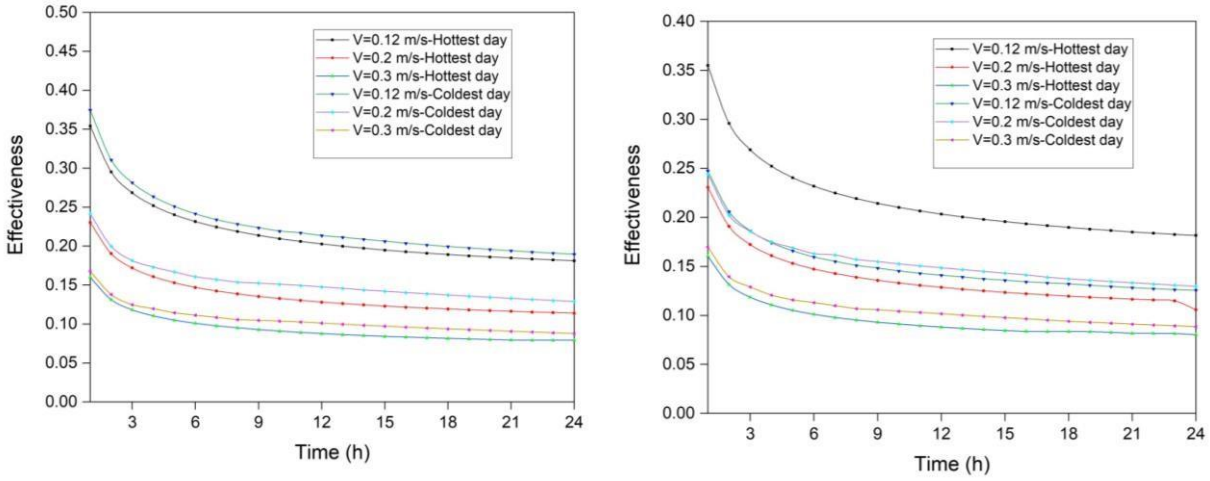

(c) (d)

Figure 18. Effectiveness with time for hottest day and coldest day with different velocity for (a) Dry Sunlight (b) Dry Sheltered (c) Wet Sunlight and (d) Wet Sheltered, inlet temperature of 311.15 K (38°C) for hottest day and 288.15 K (15 °C) for coldest day.

Figure 18 illustrates the effectiveness variation over time for the hottest and coldest days under different velocities and soil surface conditions, namely (a) Dry Sunlight, (b) Dry Sheltered, (c) Wet Sunlight, and (d) Wet Sheltered. The analysis shows that as the flow velocity increases, the effectiveness decreases. Additionally, the effectiveness for all soil surface conditions is generally low, which can be attributed to the relatively shallow depth of the U-shaped tube. However, by increasing the length of the U-shaped tube, the outlet temperature of the fluid flow can approach the undisturbed soil temperature, leading to an increase in effectiveness.

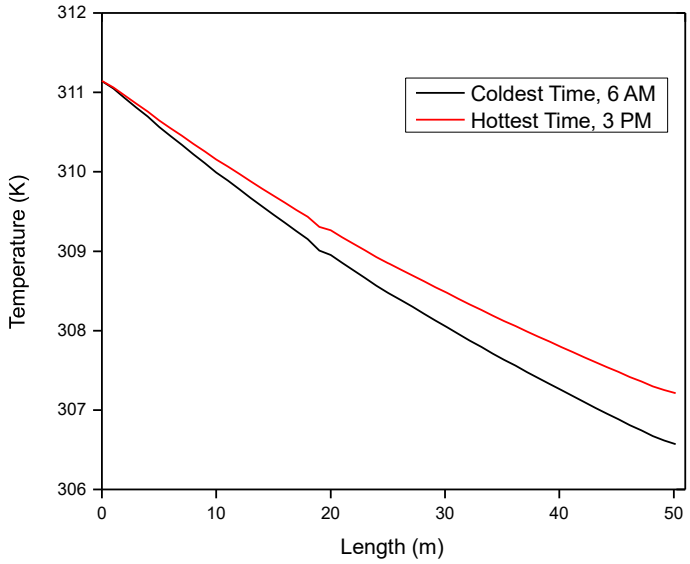

Figure 19. Temperature variation with length for dry sunlit condition inlet temperature of 311.15 K (38^{0}C) at velocity of 0.12 m/s.

Figure 19 illustrates the variation in outlet temperature along the length of the U-shaped tube in the simulation model under dry sunlit conditions. As the length of the U-shaped tube increases, there is a decrease in the outlet temperature. Specifically, when the depth of the Ushaped tube is extended from 17 m to 25 m, the reduction in outlet temperature amounts to

2.47 K and 2.22 K during the coldest and hottest times, respectively. This demonstrates that the effectiveness of the U-shaped vertical ground-coupled heat exchange is dependent on the length of the tube. As the tube length increases, the temperature difference across the tube also increases, resulting in enhanced system effectiveness.

Conclusion:

In this study, the finite volume approach in ANSYS was used to create a three-dimensional model of a vertical ground-coupled U-shaped tube heat exchanger. The model considers various soil surface conditions. The model received experimental validation to confirm its dependability and correctness. As compared to the experimental results, the transient computational fluid dynamics (CFD) simulation displayed good accuracy, with deviations of less than 2%. The transient heat transfer performance and temperature distribution properties of the vertical ground-coupled heat exchanger were examined for the fluid velocity of 0.12, 0.2, and 0.3 m/s using the validated and calibrated numerical model. The investigation led to the following important findings:

1. For coldest winter day maximum outlet temperate of GCHE is achieved with dry Sunlight surface Condition.
2. For hottest summer day minimum outlet temperate of GCHE is achieved with wet sheltered surface condition.
3. With an increase in water mass flow rate, the temperature of the water at the exit decreases in the winter and increases in the summer.
4. The mass flow rate of water influences the performance of a groundcoupled heat exchanger significantly. The effectiveness decreases as the mass flow rate increases.
5. Heat charging occurs when the borehole temperature rises rapidly near the U-shaped tube in backfill soil. The borehole loses heat in winter and gains heat in summer, making heat transfer less efficient.
6. Flow velocity increases heat transfer, but outlet temperature performance decreases. The most effective flow velocity for heat transfer and outlet temperature is 0.2 m/s.

There are additional factors that can influence the performance of the system, including various design parameters such as borehole spacing, depth, diameter, number of U-shaped tubes, U-shaped tube diameter and length, as well as the thermal conductivity, thermal diffusivity, and water content of the materials and soil. Other factors like permeability and geothermal gradient also play a role. Further research will be conducted to evaluate the collective impact of these diverse factors when multiple U-shaped tubes are installed in a single or multiple boreholes.

Declaration of competing interest

The authors of this research have stated that they did not have any competing financial interests or personal ties that could have influenced the findings presented in their work. They have made it clear that their research was conducted with complete objectivity and without any external biases.

Data availability

The data supporting the study's conclusions are included in the paper.

Acknowledgment
The author would like to thank Prof. R. V. Sharma and Prof. R. K. Prasad from the Department of Mechanical Engineering at the National Institute of Technology in Jamshedpur, INDIA, for their technical assistance. carrying out this research. **References**

[1] T. Kusuda and P. R. Achenbach, "Earth temperature and thermal diffusivity at selected stations in the United States," National Bureau of Standards Gaithersburg MD, 1965.

[2] A. K. Khatry, M. S. Sodha, and M. A. S. Malik, "Periodic variation of ground temperature with depth," *Solar Energy*, vol. 20, no. 5, pp. 425–427, 1978.

[3] G. Mihalakakou, M. Santamouris, J. O. Lewis, and D. N. Asimakopoulos, "On the application of the energy balance equation to predict ground temperature profiles," *Solar Energy*, vol. 60, no. 3–4, pp. 181–190, 1997.

[4] W. R. Herb, B. Janke, O. Mohseni, and H. G. Stefan, "Ground surface temperature simulation for different land covers," *J Hydrol (Amst)*, vol. 356, no. 3–4, pp. 327–343, 2008.

[5] M. Ouzzane, P. Eslami-Nejad, Z. Aidoun, and L. Lamarche, "Analysis of the convective heat exchange effect on the undisturbed ground temperature," *Solar Energy*, vol. 108, pp. 340–347, 2014, doi: https://doi.org/10.1016/j.solener.2014.07.015.

[6] L. R. Ingersoll, "Theory of the ground tube heat source for heat pump," *ASHVE Journal Section, Heating, Piping and Air Conditioning*, 1948.

[7] P. Eskilson, "Thermal analysis of heat extraction boreholes [Ph. D. thesis]," *Sweden: University of Lund*, 1987.

[8] M. Cimmino, M. Bernier, and F. Adams, "A contribution towards the determination of g-functions using the finite line source," *Appl Therm Eng*, vol. 51, no. 1–2, pp. 401–412, 2013.

[9] R. A. Beier, M. D. Smith, and J. D. Spitler, "Reference data sets for vertical borehole ground heat exchanger models and thermal response test analysis," *Geothermics*, vol. 40, no. 1, pp. 79–85, 2011.

[10] P. Eskilson and J. Claesson, "Simulation model for thermally interacting heat extraction boreholes," *Numerical heat transfer*, vol. 13, no. 2, pp. 149–165, 1988.

[11] G. Hellström, "Ground heat storage thermal analysis of duct storage systems. Part I. Theory," *Sweden PhD. thesis, Univ. Lund*, 1991.

[12] S. P. Kavanaugh, *SIMULATION AND EXPERIMENTAL VERIFICATION OF VERTICAL GROUND-COUPLED HEAT PUMP SYSTEMS (CLOSED LOOP)*. Oklahoma State University, 1985.

[13] T.-K. Lei, "Development of a computational model for a ground-coupled heat exchanger.," *ASHRAE, ATLANTA, GA(USA).*, no. 49–159, 1993.

[14] H. Y. Zeng, N. R. Diao, and Z. H. Fang, "A finite line‐source model for boreholes in geothermal heat exchangers," *Heat Transfer—Asian Research: Co‐sponsored by the Society of Chemical Engineers of Japan and the Heat Transfer Division of ASME*, vol. 31, no. 7, pp. 558–567, 2002.

[15] H. Zeng, N. Diao, and Z. Fang, "Heat transfer analysis of boreholes in vertical ground heat exchangers," *Int J Heat Mass Transf*, vol. 46, no. 23, pp. 4467–4481, 2003.

[16] S. Yoon, S.-R. Lee, and G.-H. Go, "A numerical and experimental approach to the estimation of borehole thermal resistance in ground heat exchangers," *Energy*, vol. 71, pp. 547–555, 2014.

[17] J. Luo, J. Rohn, M. Bayer, A. Priess, and W. Xiang, "Analysis on performance of borehole heat exchanger in a layered subsurface," *Appl Energy*, vol. 123, pp. 55–65, 2014.

[18] C. K. Lee and H. N. Lam, "Computer simulation of borehole ground heat exchangers for geothermal heat pump systems," *Renew Energy*, vol. 33, no. 6, pp. 1286–1296, 2008.

[19] D. Marcotte and P. Pasquier, "On the estimation of thermal resistance in borehole thermal conductivity test," *Renew Energy*, vol. 33, no. 11, pp. 2407–2415, 2008.

[20] B. Bouhacina, R. Saim, and H. F. Oztop, "Numerical investigation of a novel tube design for the geothermal borehole heat exchanger," *Appl Therm Eng*, vol. 79, pp. 153–162, 2015.

[21] R. Fan, Y. Jiang, Y. Yao, D. Shiming, and Z. Ma, "A study on the performance of a geothermal heat exchanger under coupled heat conduction and groundwater advection," *Energy*, vol. 32, no. 11, pp. 2199–2209, 2007.

[22] Y. Li, J. Mao, S. Geng, X. Han, and H. Zhang, "Evaluation of thermal short-circuiting and influence on thermal response test for borehole heat exchanger," *Geothermics*, vol. 50, pp. 136–147, 2014.

[23] W. Yang, M. Shi, G. Liu, and Z. Chen, "A two-region simulation model of vertical Ushaped tube ground heat exchanger and its experimental verification," *Appl Energy*, vol. 86, no. 10, pp. 2005–2012, 2009.

[24] Z. Li and M. Zheng, "Development of a numerical model for the simulation of vertical U-shaped tube ground heat exchangers," *Appl Therm Eng*, vol. 29, no. 5–6, pp. 920–924, 2009.

[25] C. Kaltreider, M. Krarti, and J. McCartney, "Heat transfer analysis of thermo-active foundations," *Energy Build*, vol. 86, pp. 492–501, 2015.

[26] A.-M. Gustafsson, L. Westerlund, and G. Hellström, "CFD-modelling of natural convection in a groundwater-filled borehole heat exchanger," *Appl Therm Eng*, vol. 30, no. 6–7, pp. 683–691, 2010.

[27] S. J. Rees and M. He, "A three-dimensional numerical model of borehole heat exchanger heat transfer and fluid flow," *Geothermics*, vol. 46, pp. 1–13, 2013.

[28] Y. Yang and M. Li, "Short-time performance of composite-medium line-source model for predicting responses of ground heat exchangers with single U-shaped tube," *International Journal of Thermal Sciences*, vol. 82, pp. 130–137, 2014.

[29] C. K. Lee, "A modified three-dimensional numerical model for predicting the shorttime-step performance of borehole ground heat exchangers," *Renew Energy*, vol. 87, pp. 618–627, 2016.

[30] I. R. Maestre, F. J. G. Gallero, P. Á. Gómez, and L. Pérez-Lombard, "A new RC and g-function hybrid model to simulate vertical ground heat exchangers," *Renew Energy*, vol. 78, pp. 631–642, 2015.

[31] A. Minaei and M. Maerefat, "Thermal resistance capacity model for short-term borehole heat exchanger simulation with non-stiff ordinary differential equations," *Geothermics*, vol. 70, pp. 260–270, 2017.

[32] A. A. Serageldin, Y. Sakata, T. Katsura, and K. Nagano, "Performance enhancement of borehole ground source heat pump using single U-shaped tube heat exchanger with a novel oval cross-section (SUO) and a novel spacer," *Sustainable Energy Technologies and Assessments*, vol. 42, p. 100805, 2020.

[33] L. Zhu, S. Chen, Y. Yang, and Y. Sun, "Transient heat transfer performance of a vertical double U-shaped tube borehole heat exchanger under different operation conditions," *Renew Energy*, vol. 131, pp. 494–505, 2019.

[34] E. D. Kerme and A. S. Fung, "Heat transfer simulation, analysis and performance study of single U-shaped tube borehole heat exchanger," *Renew Energy*, vol. 145, pp. 1430–1448, 2020.

[35] T. Kusuda and P. R. Achenbach, "Earth temperature and thermal diffusivity at selected stations in the United States," National Bureau of Standards Gaithersburg MD, 1965.